Quaternionic Local Ranking Binary Pattern: A Local Descriptor of Color Images

Rushi Lan, Yicong Zhou, *Senior Member, IEEE*, and Yuan Yan Tang, *Fellow, IEEE*

***Abstract*— This paper proposes a local descriptor called quaternionic local ranking binary pattern (QLRBP) for color images. Different from traditional descriptors that are extracted from each color channel separately or from vector representations, QLRBP works on the quaternionic representation (QR) of the color image that encodes a color pixel using a quaternion. QLRBP is able to handle all color channels directly in the quaternionic domain and include their relations simultaneously. Applying a Clifford translation to QR of the color image, QLRBP uses a reference quaternion to rank QRs of two color pixels, and performs a local binary coding on the phase of the transformed result to generate local descriptors of the color image. Experiments demonstrate that the QLRBP outperforms several state-of-the-art methods.**

***Index Terms*— Quaternionic representation (QR), local descriptor, local binary pattern (LBP), color image processing.**

I. Introduction

IMAGE descriptor is an active research topic in the fields of image processing, computer vision, and pattern recognition. A large number of image descriptors have been proposed, from the earlier Hu's geometric moment descriptor [1] and Fourier descriptor [2] to the later wavelet descriptor [3], [4], orthogonal moment invariants [5], [6], projection descriptor [7]–[9], and all kinds of local descriptors [10]–[12]. These descriptors have been successfully applied to different areas, such as image retrieval and matching [13], [14], texture classification [15], face recognition [16], and many others.

With the rapid development of modern imaging equipment and devices as well as their applications in our daily life, the demand of color image descriptors is increasing. To extract a descriptor from the color image, one strategy is to convert the color image into the corresponding gray-scale image or to simply use one color component for further processing. However, some color information has been ignored. To address this problem, another strategy is to extract the descriptor from each color component of a color image respectively or from a vector representation of the color image.

Recently, a color image representation, called *quaternionic representation (QR)*, has received numerous attentions [17]–[20]. QR encodes all color components of a pixel using a quaternion number. Compared with the RGB representation, QR has at least the following advantages: QR (1) combines all color channels of an image holistically [19], (2) achieves relatively lower computational complexity than other vector approaches [21], (3) has an implementation of vector cross correlation [22], (4) performs transformations in 3D or 4D space conveniently [23], and (5) has fruitful quaternion algebra theories which can be used in color image processing. Owing to these superiors of QR, it has been applied to many color image processing fields, like object recognition [24], synthetic-aperture radar (SAR) image analysis [25], image quality evaluation [26], and image segmentation [18].

Several image descriptors have been proposed for color images via QR. Because a quaternion can be considered as an extension of the complex number, generalizing a complex number to a quaternion number is a straightforward way to develop a quaternionic descriptor. Based on this idea, Chen *et al.* proposed the quaternionic Zernike moment descriptors which are invariant to translation and rotation transforms [27], [28]. The well-known Fourier-Mellin moment has also been extended to its quaternionic version [24]. Similar to the traditional Fourier descriptor, Mennession *et al.* proposed a geometric Fourier descriptor for image recognition [29]. Yang and Kamata developed a hypercomplex polar Fourier descriptor to analyze the color image [30]. Different from extending a complex number to a quaternion, Xu addressed the color face recognition problem using a quaternion-based discriminant analysis method [31].

However, these quaternionic image descriptors are global features of the color image. That is, they are extracted from the whole image. These descriptors generally achieved satisfactory performances when the image is with a rigid transformation (like translation, rotation, and scaling). But they do not work well when the image suffers from complicated changes (such as occlusion, illumination, or view angle variation). In this situation, more attentions should focus on local information of the original image.

The local image descriptor, as its name implies, is extracted from local regions of the image. Compared with those aforementioned global image descriptors, it is more

Manuscript received September 16, 2014; revised June 5, 2015, September 17, 2015, and December 4, 2015; accepted December 4, 2015. Date of publication December 9, 2015; date of current version December 23, 2015. This work was supported in part by the Research Committee at the University of Macau under Grant MRG001/ZYC/2013/FST, Grant MRG017/ZYC/2014/FST, Grant MYRG113(Y1-L3)-FST12-ZYC, and Grant MYRG2014-00003-FST and in part by the Macau Science and Technology Development Fund under Grant FDCT/106/2013/A3. The associate editor coordinating the review of this manuscript and approving it for publication was Prof. Jean-Philippe Thiran. *(Corresponding author: Yicong Zhou.)*

The authors are with the Department of Computer and Information Science, University of Macau, Macau 999078, China (e-mail: rslan@umac.mo; yicongzhou@umac.mo; yytang@umac.mo).

Color versions of one or more of the figures in this paper are available online at http://ieeexplore.ieee.org.

Digital Object Identifier 10.1109/TIP.2015.2507404

robust to occlusion, illumination, or view angle changes. Classical local image descriptors include scale-invariant feature transform (SIFT) [10], gradient location-orientation histogram (GLOH) [32], speeded up robust features (SURF) [11], local binary pattern (LBP) [33], histograms of oriented gradient (HOG) descriptor [34], GA-SIFT [35], and Weber local descriptor (WLD) [36], [37], etc. For color images, these descriptors are extracted from the HSV channels [38], [39], opponent color space, RGB channels, and filtering domain [40], [41]. Promising results have been achieved in this field. More details about these descriptors can be found in [32], [42], and [43].

Although QR has several attractive metrics in color image processing, to the best of our knowledge, extracting a local descriptor of a color image directly in the quaternionic domain has not been addressed yet. Unlike the aforementioned extraction strategies of local color image descriptors, our efforts in this work focus on developing the local descriptor using QR. In this way, the obtained descriptor will not only take the advantages of QR but also represent robust local characteristics of the color image.

In this paper, we propose a novel local descriptor, named *quaternionic local ranking binary pattern (QLRBP)*, for color images. QLRBP is based on QR of the color image and treats all color channels in a holistic way. It not only reveals the stereo characteristics of the original color image but also possesses robustness to different variations. After analyzing LBP and its improvements, we come out a new perspective that these methods can be converted into a scheme of designing a proper ranking function to determine the ordering between two pixels. In QLRBP, to propose a quaternionic ranking function, a Clifford translation of quaternion (CTQ) is applied to QR of the color image such that the phase of the CTQ result is able to determine the order of two color pixels and its physical meaning is easily interpreted. The LBP coding is then applied to the phase image to obtain a QLRBP coding image, from which we extract the dense local histograms as the local image descriptor. Moreover, the properties of CTQ is also deeply studied. The proposed QLRBP is evaluated by the person reidentification and face recognition problems. Comparison results show the effectiveness of QLRBP.

The remaining of this paper is structured as follows. Some background knowledge is given in Section II. The properties of CTQ and comparisons with rotation of quaternion (ROQ) are presented in Section III. Our new understanding of LBP based methods is given in Section IV. The proposed QLRBP is introduced detailedly in Section V. Experiments are provided to evaluate QLRBP in Section VI, and a conclusion is finally given in Section VII.

II. Quaternion and Quaternionic Representation

This section presents related background knowledge, including quaternion algebra, weighted L_1 phase for quaternions, and quaternionic representation (QR).

A. Quaternion Algebra

The quaternion, first introduced by Hamilton in 1843 [44], is a four-dimensional generation of the complex number. It has one real part and three imaginary parts. A quaternion $\dot{q} \in \mathbb{H}$ can be represented in a complex form as follows:

$$\dot{q} = a + ib + jc + kd, \tag{1}$$

where a, b, c and d are real numbers, i, j and k are complex operators, satisfying:

$$i^2 = j^2 = k^2 = ijk = -1.$$

a is called the real part of a quaternion, and $ib + jc + kd$ is the imaginary part. Denoting the real and imaginary parts as $S(\dot{q})$ and $V(\dot{q})$ respectively, we have $\dot{q} = S(\dot{q}) + V(\dot{q})$.

Several properties of complex numbers have been extended to the quaternion as follows:

- Conjugate: $\dot{q}^* = a - (ib + jc + kd)$;
- A pure quaternion: $\dot{q} = ib + jc + kd$;
- Modulus: $|\dot{q}| = \sqrt{\dot{q}\dot{q}^*} = \sqrt{\dot{q}^*\dot{q}} = \sqrt{a^2 + b^2 + c^2 + d^2}$;
- A unit quaternion: $|\dot{q}| = 1$;
- Inverse: $\dot{q}^{-1} = \frac{\dot{q}^*}{|\dot{q}|^2}$ so that $\dot{q}\dot{q}^{-1} = 1$;
- Modulus of multiplication: $\forall \dot{q}_1, \dot{q}_2 \in \mathbb{H}$, $|\dot{q}_1\dot{q}_2| = |\dot{q}_1||\dot{q}_2|$.

As a complex number, a quaternion can also be represented in the polar form:

$$\dot{q} = |\dot{q}|e^{\dot{\mu}\theta} = |\dot{q}|(\cos\theta + \dot{\mu}\sin\theta), \tag{2}$$

where $\dot{\mu}$ is a unit pure quaternion. Note that the definition of four quadrant arctangent is used to calculate θ such that $0 \leqslant \theta \leqslant \pi$. $\dot{\mu}$ and θ are known as the eigenaxis and phase (or eigenangle) of the quaternion, which can be obtained by:

$$\dot{\mu} = \frac{V(\dot{q})}{|V(\dot{q})|} = \frac{ib + jc + kd}{\sqrt{b^2 + c^2 + d^2}}, \tag{3}$$

$$\theta = \tan^{-1}\frac{|V(\dot{q})|}{S(\dot{q})} = \tan^{-1}\frac{\sqrt{b^2 + c^2 + d^2}}{a}. \tag{4}$$

Based on the definition and properties of the quaternion, several operators have been proposed. Two well-known operators, rotation of quaternion (ROQ) and Clifford translation of quaternion (CTQ), are briefly introduced in the following.

1) ROQ: Rotation is an important operator of the quaternion. Its definition is given as follows.

Definition 1 (Rotation of Quaternion): The rotation of a quaternion $\dot{q}$ by a unit quaternion $\dot{p}$ is defined by:

$$\mathrm{ROQ}(\dot{q}, \dot{p}) = \dot{p}\dot{q}\dot{p}^*. \tag{5}$$

After rotation, the real part of $\dot{q}$ does not change, but its imaginary part is rotated in a three-dimensional (3D) space. Besides, the modulus and phase of $\mathrm{ROQ}(\dot{q}, \dot{p})$ and $\dot{q}$ are the same.

2) CTQ: CTQ is an isometric mapping of a quaternion that multiplies a quaternion with a unit quaternion. Its definition is given as follows [45]:

Definition 2 (Clifford Translation of Quaternion): Suppose $\dot{q}$ is a quaternion, and $\dot{p}$ is a unit quaternion. The right and left Clifford translations of $\dot{q}$ by $\dot{p}$ are defined as follows respectively:

$$\mathrm{CTQ}_r(\dot{q}, \dot{p}) = \dot{q}\dot{p} \quad \text{and } \mathrm{CTQ}_l(\dot{q}, \dot{p}) = \dot{p}\dot{q}.$$

ROQ has been applied to various applications of color image processing because we can easily perform a transformation to a color pixel in the color space [45]. Based on ROQ, several quaternionic distances have been proposed to detect impulse noise in a color image. However, few attentions have been paid on CTQ. In this work, we will further study its properties and use CTQ to derive a novel local descriptor.

B. Weighted L_1 Phase for Quaternions

The phase, defined in Eq. (4), describes the relationship between the real and imaginary parts of $\dot{q}$. The L_2-norm of imaginary coefficients (b, c, d) is used. It is well-known that the L_1-norm has been widely applied to many applications because of its simplicity and robustness to outliers and small noise. In this work, we extend the original phase using L_1-norm and propose a novel weighted L_1 phase for $\dot{q}$ as follows:

$$\delta = \tan^{-1} \frac{\alpha_1|b| + \alpha_2|c| + \alpha_3|d|}{a} = \tan^{-1} \frac{\boldsymbol{\omega}^T \boldsymbol{\beta}}{a}, \tag{6}$$

where $\boldsymbol{\omega} = (\alpha_1, \alpha_2, \alpha_3)^T$ denotes the weight vector, and $\boldsymbol{\beta} = (|b|, |c|, |d|)^T$. If $\boldsymbol{\omega} = (1, 1, 1)^T$, $\boldsymbol{\omega}^T \boldsymbol{\beta}$ is the L_1-norm of (b, c, d). There are at least two advantages to introduce $\boldsymbol{\omega}$ in Eq. (6). First, it can be used to accommodate the importance of a specific imaginary component. Second, we can change the value range of δ by choosing a proper $\boldsymbol{\omega}$.

C. QR of Color Image

In literature, the imaginary part of a quaternion is used to represent a color pixel in an image, namely

$$\dot{q} = ir + jg + kb, \tag{7}$$

where r, g, and b are the red, green, and blue components of a color pixel respectively. QR of a color image in Eq. (7) gives a one-to-one mapping between the quaternionic space and RGB color space. Therefore, quaternionic operators, including modulus, phase, ROQ and CTQ, are able to process the color image in a holistic way.

III. Analysis of CTQ

A remarkable feature of CTQ is that the distance between a quaternion and its CTQ one is the same for every quaternion. That is, $|\dot{q} - \mathrm{CTQ}(\dot{q}, \dot{p})|$ is fixed for each $\dot{q} \in \mathbb{H}$. In this section, we deeply study the properties of CTQ and then compare it with ROQ.

A. Properties of CTQ

Based on the definition of CTQ and properties of the quaternion, we can derive the following properties of CTQ. The proofs of these properties are presented in Appendix.

Property 1: CTQ does not change the modulus of the quaternion, namely

$$|\mathrm{CTQ}_r(\dot{q}, \dot{p})| = |\mathrm{CTQ}_l(\dot{q}, \dot{p})| = |\dot{q}|. \tag{8}$$

TABLE I
Comparison of ROQ and CTQ

	ROQ	CTQ
Real Part	*Invariant*	***Changed***
Imaginary Part	*Changed*	*Changed*
Modulus	*Invariant*	*Invariant*
Phase	*Invariant*	***Changed***

Property 2: CTQ does not satisfy the noncomutativity of multiplication, that is, $\mathrm{CTQ}_r(\dot{q}, \dot{p})$ is not equal to $\mathrm{CTQ}_l(\dot{q}, \dot{p})$, but their phases are the same, namely

$$\theta_{\mathrm{CTQ}_r(\dot{q},\dot{p})} = \theta_{\mathrm{CTQ}_l(\dot{q},\dot{p})}. \tag{9}$$

For simplicity, we use $\theta_{\mathrm{CTQ}(\dot{q},\dot{p})}$ to represent the phase of the right or left CTQ of $\dot{q}$ by $\dot{p}$ in the rest of this paper.

Property 3: The rotation of a quaternion $\dot{q}$ along with another unit quaternion $\dot{p}$ can be obtained by a combination of left and right CTQs of $\dot{q}$ and $\dot{p}$ as follows:

$$\begin{aligned} \mathrm{ROQ}(\dot{q}, \dot{p}) &= \mathrm{CTQ}_r(\mathrm{CTQ}_l(\dot{q}, \dot{p}), \dot{p}^*) \\ &= \mathrm{CTQ}_l(\mathrm{CTQ}_r(\dot{q}, \dot{p}^*), \dot{p}). \end{aligned} \tag{10}$$

Property 4: If $\dot{q}$ and $\dot{p}$ are pure quaternions, the right CTQ of $\dot{q}$ by $\dot{p}$ is equivalent to its conjugate of the left CTQ, namely

$$\mathrm{CTQ}_r(\dot{q}, \dot{p}) = \mathrm{CTQ}_l(\dot{q}, \dot{p})^*. \tag{11}$$

Property 5: If $\dot{q}$ and $\dot{p}$ are both pure quaternions, the weighted L_1 phases of $\mathrm{CTQ}_r(\dot{q}, \dot{p})$ and $\mathrm{CTQ}_l(\dot{q}, \dot{p})$ are the same, namely

$$\delta_{\mathrm{CTQ}_r(\dot{q},\dot{p})} = \delta_{\mathrm{CTQ}_l(\dot{q},\dot{p})}. \tag{12}$$

B. ROQ Versus CTQ

As aforementioned, both ROQ and CTQ are transformations of a quaternion. They are related to each other but not exactly the same. Table I compares them from the following aspects: real part, imaginary part, modulus, and phase. ROQ and CTQ change the imaginary part of a quaternion while keeping the modulus invariant. On the other hand, CTQ changes the real part and phase of a quaternion, but ROQ does not.

IV. Ranking Based LBPs

In this section, we introduce our new understanding of LBP-based methods from the perspective of ranking. To begin with, the definition of basic LBP is presented.

A. Local Binary Pattern (LBP)

Local binary pattern (LBP), first proposed by Ojala *et al.* [33], is a simple but efficient tool to describe local information within an image. The local differences in an image can be decomposed into two parts: the sign and magnitude [15]. The traditional LBP makes use of the sign part to code the local pattern as an 8-digit binary number. It is usually converted to a decimal number for convenience. Let x_m be the center pixel of a 3×3 block S_m within

a grayscale image, the LBP coding is obtained by comparing x_m with its surrounding pixels as follows:

$$\mathrm{LBP}_{x_m} = \sum_{n=0}^{|S_m|-1} h(x_n - x_m)2^n, \quad h(t) = \begin{cases} 1, & t \geqslant 0. \\ 0, & t < 0. \end{cases} \tag{13}$$

where $|S_m|$ is the number of elements in S_m. A histogram can be computed over an image cell and used as features of the image. LBP has been successfully adapted to numerous applications, like texture classification, face recognition, and shape localization.

B. Ranking Based LBPs

Observing Eq. (13), we can find that 1 and 0 can be considered as a simple *ordering* relationship between x_m and x_n. 1 means that x_n is in front of x_m, otherwise x_n is behind x_m. This ordering relationship is determined by a combination of $x_n - x_m$ and $h(t)$.

In Eq. (13), $x_n - x_m$ can be considered as a mapping of x_m and x_n. To extend $x_n - x_m$ into a more general form and to mathematically describe their ordering relationship, we introduce a *ranking function* of x_m and x_n as following:

$$R(x_m, x_n) = f(x_m, x_n) - T, \tag{14}$$

where $R(x_m, x_n)$ is a ranking function and gives an exact ordering relationship. If x_n is ranked higher than x_m, $R(x_m, x_n) \geqslant 0$, else $R(x_m, x_n) < 0$. $f(x_m, x_n)$ is a mapping function of x_m and x_n, and T is a threshold. Then Eq. (13) turns to

$$\bar{h}(x_m, x_n) = \begin{cases} 1, & \text{if } R(x_m, x_n) \geqslant 0, \\ 0, & \text{if } R(x_m, x_n) < 0. \end{cases} \tag{15}$$

Now we are able to analyze LBP and several its improvements from the viewpoint of ranking. In LBP, we have

$$R_{\mathrm{LBP}}(x_m, x_n) = x_n - x_m. \tag{16}$$

The completed LBP (CLBP) encodes the magnitude of $x_n - x_m$ [15]. Its corresponding ranking function is:

$$R_{\mathrm{CLBP}}(x_m, x_n) = |x_n - x_m| - c, \tag{17}$$

where c is the mean value of $|x_n - x_m|$ for the whole image. Similarly, we can also derive the ranking function for the well-known local ternary pattern (LTP) [46]. LTP can be split into the upper LBP (ULBP) and lower LBP (LLBP). Their corresponding ranking functions are:

$$R_{\mathrm{ULBP}}(x_m, x_n) = x_n - x_m - c_1, \tag{18}$$

$$R_{\mathrm{LLBP}}(x_m, x_n) = x_m - x_n - c_2, \tag{19}$$

where c_1 and c_2 are two given thresholds.

The aforementioned LBP, CLBP, ULBP and LLBP were proposed for gray-scale images. Considering color images, Lee *et al.* proposed a local color vector binary pattern (LCVBP) for color face recognition [16]. Let $x_m = (r_m, g_m, b_m)^T$ and $x_n = (r_n, g_n, b_n)^T$ be two color pixels. The corresponding ranking functions for LCVBP are:

$$R_{\mathrm{LCVBP}_1}(x_m, x_n) = \sqrt{r_n^2 + g_n^2 + b_n^2} - \sqrt{r_m^2 + g_m^2 + b_m^2}, \tag{20}$$

$$R_{\mathrm{LCVBP}_2}(x_m, x_n) = \tan^{-1}\frac{r_n}{b_n} - \tan^{-1}\frac{r_m}{b_m}. \tag{21}$$

In Eq. (21), $\frac{r_n}{b_n}$ and $\frac{r_m}{b_m}$ can be replaced by other color channels.

Observing Eqs. (16) to (21), LBP-based methods have different ranking functions that determine the performances of these methods. Different ranking functions are able to exhibit local information of an image from various perspectives. For example, Eq. (16) ranks x_m and x_n directly by their difference, while Eq. (18) makes an improvement by translating their difference with c_1 to obtain another coding result. Therefore, we can improve LBP-based methods by designing a better ranking function $R(x_m, x_n)$.

V. Quaternionic Local Ranking Binary Pattern

This section introduces QLRBP as a new local descriptor in detail. As aforementioned, the key step in the LBP-based method is to design a proper ranking function. Therefore, we first discuss the ranking of two quaternions.

A. Direct Ranking of Two Quaternions

Suppose $\dot{q_m}$ and $\dot{q_n}$ are QRs of two pixels in a color image. An intuitive way is to use the modulus of the difference between $\dot{q}_m$ and $\dot{q}_n$ to build their ranking function, namely

$$R_{\mathrm{M}_1}(\dot{q_m}, \dot{q_n}) = |\dot{q_n} - \dot{q_m}| - T. \tag{22}$$

Because $|\dot{q_n} - \dot{q_m}| \geqslant 0$, it is difficult to find an appropriate threshold T to determine the ranking of two quaternions.

Rewriting Eq. (22), we can obtain another version of $R_{\mathrm{M}_1}(\dot{q_m}, \dot{q_n})$ to compare the modulus of two quaternions as follows:

$$R_{\mathrm{M}_2}(\dot{q_m}, \dot{q_n}) = |\dot{q_n}| - |\dot{q_m}|. \tag{23}$$

According to the definition of the quaternion's modulus, $|\dot{q_n}|$ and $|\dot{q_m}|$ are the magnitudes of two pixels in the color space. Therefore, Eq. (23) is a measure of the difference between $\dot{q}_n$ and $\dot{q}_m$ in the color space. Thus, it can be applied to rank them. Actually, Eq. (23) is equivalent to Eq. (20) used in LCVBP. But $R_{\mathrm{M}_2}(\dot{q}_m, \dot{q}_n)$ in Eq. (23) lacks of the discriminative ability. For example, when $\dot{q}_1 = i, \dot{q}_2 = j, \dot{q}_3 = k$, we have

$$R_{\mathrm{M}_2}(\dot{q}_1, \dot{q}_2) = R_{\mathrm{M}_2}(\dot{q}_1, \dot{q}_3) = R_{\mathrm{M}_2}(\dot{q}_2, \dot{q}_3) = 0. \tag{24}$$

We cannot make any ranking decision for $\dot{q}_1, \dot{q}_2$, and $\dot{q}_3$ when considering only the difference of their moduli.

Apart from the modulus, the phase of the quaternion can also be used to derive the ranking function because it reveals the relationship between the real and imaginary parts of a quaternion. However, if we apply QR of a color image as shown in Eq. (7), the phase will be equal to $\frac{\pi}{2}$ for all pixels. To avoid this problem, QR could be proposed in other ways, such as $r + ig + jb$, but this also lacks of the discriminative ability.

B. Quaternionic Ranking With CTQ

From above analysis, it is difficult to derive an appropriate ranking function when directly considering the modulus or phase of a quaternion. In order to overcome this obstacle, we introduce a third quaternion, named the *reference quaternion*,

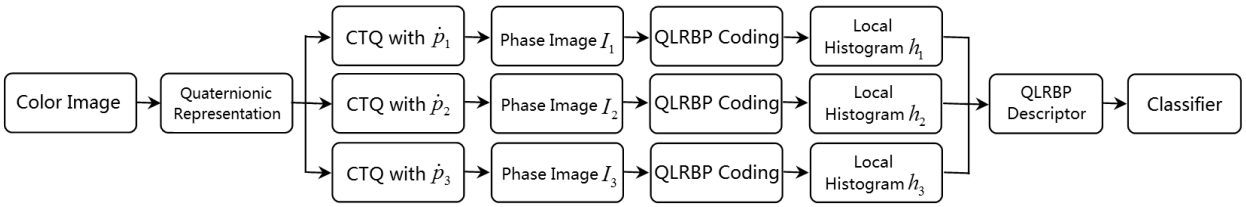

Fig. 1. The framework of QLRBP.

to perform a transformation to two quaternions, and then rank them according to their new phases or moduli. There are at least two advantages using a reference quaternion:

1) We can obtain an explicit ranking decision for two quaternions transformed by a given reference quaternion;
2) Changing the reference quaternion yields a different ranking decision.

Because rotation is a commonly used operator for color image processing, we can rotate two quaternions towards the reference quaternion. However, it cannot achieve above purposes because the modulus and phase of a quaternion keep the same after rotation. Therefore, we need to find another proper operator to rank two quaternions. Here, we propose to rank two quaternions using CTQ. Because CTQ keeps the modulus of the quaternion unchanged (See Table I), the phase of CTQ is then used to rank the quaternions.

Without loss of generality, let $\dot{q} = ir + jg + kb$ and $\dot{p} = ir' + jg' + kb'$, where r, r', g, g', b, and b' are intensity values of the red, green, and blue components respectively, and the reference quaternion $\dot{p}$ is a unit pure quaternion. From Property 2 of CTQ given in Section III-A, the phases of left and right CTQs of a quaternion are equal. Therefore, the right CTQ of $\dot{q}$ by $\dot{p}$ is used as an example here.

$$\begin{aligned} \mathrm{CTQ}_r(\dot{q}, \dot{p}) &= (ir + jg + kb)(ir' + jg' + kb') \\ &= -(rr' + gg' + bb') + i(gb' - bg') \\ &\quad + j(br' - rb') + k(rg' - gr'). \end{aligned} \tag{25}$$

Then the phase of $\mathrm{CTQ}_r(\dot{q}, \dot{p})$ is

$$\theta = \tan^{-1} \frac{\sqrt{(gb' - bg')^2 + (br' - rb')^2 + (rg' - gr')^2}}{-(rr' + gg' + bb')}. \tag{26}$$

Observing the denominator of Eq. (26), we can find that it is actually the inner product of two vectors, $(r, g, b)^T$ and $(r', g', b')^T$, which are the color components of two pixels. If the quaternion $\dot{q}$ is close to the reference one $\dot{p}$, their inner product will be large. On the other hand, the numerator of Eq. (26) contains three parts, each of which is the difference of cross multiplications of two components of $\dot{q}$ and $\dot{p}$. As a result, if $\dot{q}$ and $\dot{p}$ are similar to each other, the phase of $\mathrm{CTQ}_r(\dot{q}, \dot{p})$ will be large and can be regarded as a measure of the similarity of two quaternions. This similarity contains a specific characteristic of $\dot{q}$, and it is determined by $\dot{p}$. It is possible to obtain a certain shape or region whose major color component is close to $\dot{p}$. For instance, if $\dot{p}$ is set to i, the proportion of red component of $\dot{q}$ is extracted. Similarly, the luminance feature of the image can be emphasized by choosing the gray axis of RGB space $\frac{i+j+k}{\sqrt{3}}$ as the reference quaternion [19].

From Eq. (26) we can see that the difference of cross multiplications of two components of $\dot{q}$ and $\dot{p}$ is set to the same weight. Actually, different color channels of the color image contain various visual information, and should be handled on its merits. For example, when converting a color image into a gray-scale image, we give different weights to the red, green, and blue components. To adaptively accommodate the importance of specific components, the weighted L_1 phase defined in Eq. (6) is used here:

$$\delta = \tan^{-1} \frac{\alpha_1 |gb' - bg'| + \alpha_2 |br' - rb'| + \alpha_3 |rg' - gr'|}{-(rr' + gg' + bb')}. \tag{27}$$

The above equation is a weighted version of Eq. (26). By setting α_1, α_2 and α_3 with different values, the differences of corresponding color components can be highlighted.

Now, to rank two quaternions $\dot{q}_m$ and $\dot{q}_n$, we first perform a CTQ to them by a given reference $\dot{p}_1$, and then make a ranking decision according to the phase given in Eq. (27) of two CTQ quaternions. The ranking function can be expressed as

$$R_{\mathrm{QLRBP}}(\dot{q}_m, \dot{q}_n) = \delta_{\mathrm{CTQ}(\dot{q}_n, \dot{p}_1)} - \delta_{\mathrm{CTQ}(\dot{q}_m, \dot{p}_1)}. \tag{28}$$

From Section III-B, choosing another reference quaternion will change the value of $\delta_{\mathrm{CTQ}(\dot{q}_n, \dot{p}_1)}$. As a result, it is possible to achieve different ranking results of $\dot{q}_m$ and $\dot{q}_n$ using different reference quaternions. This may help to understand the content of an image from different perspectives.

Based on the quaternionic ranking introduced here, we can obtain the framework of QLRBP as illustrated in Fig. 1. CTQ is performed to QR of a color image with different reference quaternions $\dot{p}_t$ $(t = 1, 2, 3)$, then the phase images are calculated to rank neighboring pixels. The following subsections will introduce the remaining steps to derive the QLRBP descriptor.

C. QLRBP Coding

Based on QR and the ranking function in Eq. (28), we can derive the definition of the QLRBP coding. Considering an image pixel $\dot{q}_m$ centered in a 3×3 block S_m and a specified reference quaternion $\dot{p}_1$, the QLRBP coding is calculated by:

$$\mathrm{QLRBP}_{\dot{q}_m} = \sum_{n=0}^{|S_m|-1} h(R_{\mathrm{QLRBP}}(\dot{q}_m, \dot{q}_n)) 2^n, \tag{29}$$

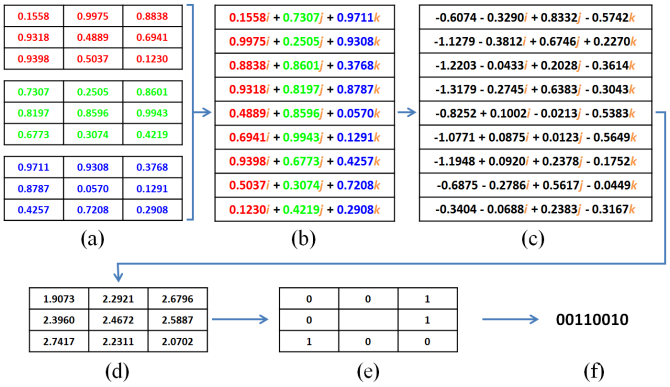

Fig. 2. Example of QLRBP coding. (a) The input 3×3 image patches for red, green, and blue channels respectively. (b) The QRs of all color pixels. (c) The CTQ results of all pixels. The reference quaternion $\dot{p} = 0.8815i + 0.4489j + 0.1463k$. (d) The weighted L_1 phases of the CTQ results in (c). All weights are set to 1. (e) The ranking results between the center pixel and its surrounding ones. (f) The binary string obtained from the ranking results.

where $|S_m|$ is the number of elements in S_m, $h(\cdot)$ and $R_{\text{QLRBP}}(\dot{q}_m, \dot{q}_n)$ are defined in Eqs. (13) and (28), respectively. Fig. 2 presents an illustrative example to show the detailed implementation of QLRBP in a local region of a color image.

A grayscale image can be obtained from Eq. (29). Its contents are dependent on $R_{\text{QLRBP}}(\dot{q}_m, \dot{q}_n)$ directly. If we use another reference quaternion, this grayscale image will be changed because the value of $R_{\text{QLRBP}}(\dot{q}_m, \dot{q}_n)$ may differ. To extract comprehensive information from the original image, a number of reference quaternions $\{\dot{p}_1, \dot{p}_2, \cdots, \dot{p}_L\}$ are utilized to perform QLRBP coding, and then concatenating these QLRBP features generates the final descriptors.

D. Feature Representation Using QLRBP

Similar to most LBP-based methods, the histogram of the QLRBP coding image is used as features for recognition. In order to obtain more robust features against variations of illumination, view angle, pose, and occlusion, the histogram is extracted from overlapping cells like other dense local descriptors. The centers of all cells are uniformly distributed within the image. A normalization is then performed to the histograms of all cells. Finally, concatenating the normalized histograms generates the QLRBP feature representation of the original color image. The detailed steps of the QLRBP feature extraction are given in Algorithm 1.

E. Reference Quaternion Selection Methods

In QLRBP, we rank the center quaternion and its surrounding ones. Different reference quaternions will yield different ranking results. Here, we discuss how to find an appropriate reference quaternion for QLRBP.

It is unnecessary to use a large number of reference quaternions for the QLRBP coding. The reason mainly lies in that, if two reference quaternions are close, their coding results will be similar. Moreover, a large number of reference quaternions will result in great redundancy between the coding results. Thus, the selected reference quaternions should obtain different coding results while being uncorrelated with each other. Because a color image has three color channels, we select three reference quaternions for QLRBP.

Algorithm 1 QLRBP Feature Extraction

Input: The color image I, a reference quaternion set $\{p_1, p_2, \cdots, p_L\}$, and the sidelength of the local cell d.

- Step 1: Represent all pixels of I using Eq. (2). Denote the quaternionic image as Q_I.
- Step 2: For $i = 1$ to L, do
  - (a) Perform CTQ to all elements of Q_I by p_i, then calculate the phase image of the Clifford translated image $\text{CTQ}(Q_I, p_i)$ according to Eq. (27).
  - (b) Perform the QLRBP coding according to Eqs. (28) and (29).
  - (c) Divide the QLRBP coding image into several overlapping cells according to the sidelength d.
  - (d) Calculate the normalized histogram of each cell. List all histograms together to achieve a feature vector f_i.

Output: The QLRBP feature vector of I: $\{f_1, f_2, \cdots, f_L\}$.

As aforementioned, the phase of the CTQ result can be used to describe the similarity between QR of the color pixel and a reference quaternion. From the perspective of feature extraction, the reference quaternions should be representative ones to show the color distribution of an image, and be distinctive from each other. Each reference quaternion can be considered as a codeword here, and all of them form a codebook. Inspired by existing codeword generation methods [47], [48], we design reference quaternions in two manners: learning-based and hand-crafted methods.

Learning-based methods apply the data clustering algorithms to find three clusters from the original image, and choose these clusters as reference quaternions. The clusters derived by different methods reveal the color distribution of an image from different aspects. Following this idea, we develop following ways to derive reference quaternions:

1) Encode a color image using the vector representation, and apply the K-means algorithm to find clusters as the reference quaternions.
2) Based on QR of the color image, utilize the binary quaternion-moment-preserving (BQMP) thresholding technique [18] to find three representative quaternions as the reference quaternions.

The first scheme searches the clusters in a 3D vector space, while the latter one works in the quaternionic domain. They both determine the reference quaternions according to image contents. The obtained reference quaternions will adaptively change with different images.

Although the learning-based methods have several advantages, they usually have high computation complexity. Here we also develop hand-crafted reference quaternions to achieve higher efficiency. The complex operators, i, j, and k, play key roles in the quaternion space because any pure quaternion can be represented by their linear combinations. However, if we select the reference quaternion with only one complex operator, namely two elements of (r', g', b') in Eq. (27) are set to zero, relationships between color channels will be ignored. Therefore, we apply small random movements to the complex

operators as follows:

$$\begin{pmatrix} i_1 \\ j_1 \\ k_1 \end{pmatrix} = \begin{pmatrix} 1-\epsilon_{11} & \epsilon_{12} & \epsilon_{13} \\ \epsilon_{21} & 1-\epsilon_{22} & \epsilon_{23} \\ \epsilon_{31} & \epsilon_{32} & 1-\epsilon_{33} \end{pmatrix} \begin{pmatrix} i \\ j \\ k \end{pmatrix}, \quad (30)$$

where random number $\epsilon_{mn} \in [0, 0.1]$, $\{i_1, j_1, k_1\}$ are small variants of $\{i, j, k\}$. Their directions are almost orthogonal to each other in the 3D space. Although ϵ_{mn} is set to a small value, it helps to preserve interactions between color channels. In the coming section, we will carry out experiments to evaluate these proposed reference quaternions.

F. Discussion

In this section, we have detailedly introduced our QLRBP. Compared with several existing LBP-based approaches which process all color channels individually, the proposed QLRBP has the following advantages.

1) QLRBP is based on QR of the color image. The red, green, and blue components are three basic attributions of a color image. It is possible to obtain more robust features by considering the relations between different color channels [16]. Encoding all color channels together, QR offers a flexible way to handle them at the same time. Several quaternionic operators can be used to analyze the color image in the quaternionic space. Therefore, the relations between different color channels are considered and rich information can be extracted from the original color image.
2) CTQ is used in QLRBP. Finding a proper operator for QR of the color image is a key problem. As a normal operator in quaternion algebra, CTQ is the first time to be applied for color image processing. Each portion of the CTQ result has its specific meaning in the original color space, i.e. the real part describes the similarity of all color channels of two pixels, while the imaginary part consists of the differences between two different color channels (see Eq. (25)). Applying CTQ to the color image with different quaternions, the obtained features will differ.
3) Observing the procedures of QLRBP and LCVBP, we can find that they both consider the relationships between color channels rather than handling each channel individually. However, QLRBP achieves more superiorities than LCVBP. First, LCVBP considers only two color channels, while QLRBP takes all three color channels into account at one time. Second, LCVBP utilizes two color channels in a straightforward manner. However, QLRBP introduces a reference quaternion and describes the relationships of all three color channels with respect to the reference quaternion. This provides users the flexibility of obtaining different characteristics of the color image by choosing the corresponding reference quaternion. Third, QLRBP considers more comprehensive relationships of color channels than LCVBP. Eq. (21) indicates that the ratio of two color channels is directly used to derive LCVBP. As shown in Eq. (27), QLRBP uses the color channel differences and the similarity between the color pixel and the reference quaternion.

Due to the above superiorities, QLRBP is able to extract more discriminative information of the color image than several existing LBP-based methods.

VI. Experimental Results

This section provides several experimental results to demonstrate the effectiveness of the proposed QLRBP. After selecting proper parameters for QLRBP, we evaluate QLRBP using two challenging problems, person reidentification and face recognition.

A. Parameter Selection

QLRBP has two types of parameters: reference quaternions and weights to calculate the phase. We first study the performances of different reference quaternions using fixed weights. Once the optimal reference quaternions are chosen, the effects of various weights will be investigated.

1) Selection of Reference Quaternions: Four generation schemes of reference quaternions have been introduced in Section V-E, i.e. two learning-based methods, $\{i, j, k\}$, and $\{i_1, j_1, k_1\}$. Denote these reference quaternions as ReQ_1, ReQ_2, ReQ_3 and ReQ_4, and their corresponding descriptors as QLRBP_1, QLRBP_2, QLRBP_3, and QLRBP_4 respectively. In this paper, ReQ_4 is selected as: $i_1 = 0.9922i + 0.0857j + 0.0907k$, $j_1 = 0.0912i + 0.9908j + 0.0999k$, and $k_1 = 0.0852i + 0.0855j + 0.9927k$. We evaluate the performances of these reference quaternions by setting the weights to $\{1, 1, 1\}$.

The first image in Fig. 6 is used as an example to show the effectiveness of different reference quaternions. After QR, we perform CTQ using four reference quaternions, compute their phases using Eq. (27), and apply the QLRBP coding to them respectively. The results are shown in Fig. 3, in which the images in each row represent the results of one reference quaternion. The first three images in each row are phase images while the remaining three images are the QLRBP coding images. Observing the phase images in Fig. 3, we can find that there is a shape of the person in each phase image. The phase images are similar to each other if they are obtained by the same reference quaternion, e.g. three phase images obtained by ReQ_1 in the first row in Fig. 3. However, the phase images obtained by different methods look different. As a result, different reference quaternions yield different phase images. Different color features of the original image can be used to describe the local information of a color image.

Fig. 3 also shows the QLRBP coding images using different reference quaternions, but we cannot obtain any visual features from them. Instead, we analyze the QLRBP coding images in a quantitive way. Inspired by the Fisher's linear discriminant, we hope the proposed descriptors, derived from different reference quaternions, have large similarity within the same class and little similarity between different classes. To evaluate the proposed descriptors from this view-point, we calculate the similarity of the person images within and between classes. Two datasets of person images, i.e. ETHZ[1] [49] and i-LIDS

[1] http://www.umiacs.umd.edu/~schwartz/datasets.html.

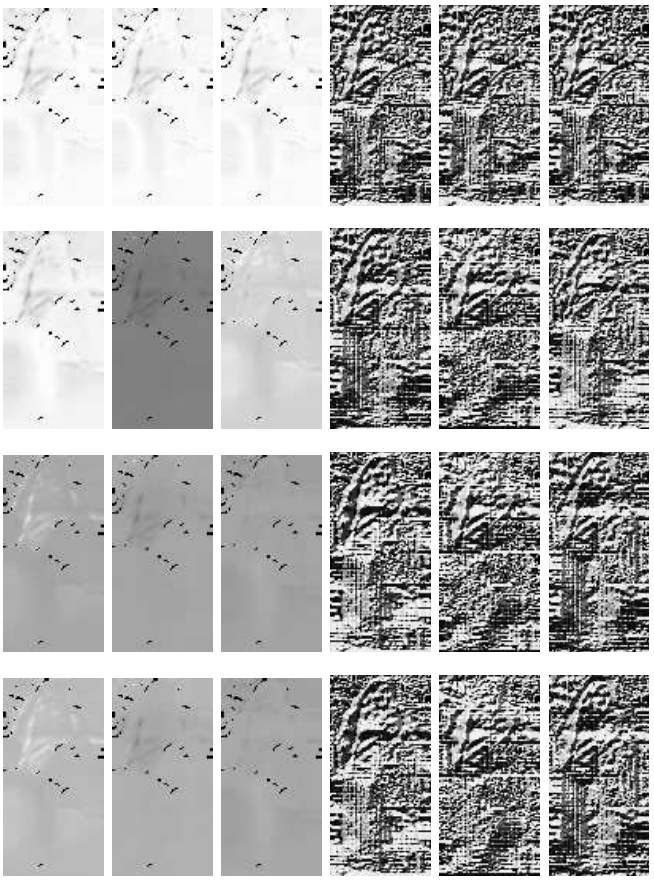

Fig. 3. Phase images and their corresponding QLRBP coding results of the first image in Fig. 6 using different reference quaternions. The 1st - 4th rows show the results using ReQ_1, ReQ_2, ReQ_3 and ReQ_4, respectively. In each row, the first three images are phase images and other three are the QLRBP coding results.

TABLE II
AVERAGE SIMILARITIES OF THE QLRBP FEATURES DERIVED BY DIFFERENT REFERENCE QUATERNIONS

	QLRBP_1	QLRBP_2	QLRBP_3	QLRBP_4
Υ_w	0.7434	0.7191	0.7441	**0.7463**
Υ_b	0.6571	**0.6320**	0.6366	0.6369
Υ_w/Υ_b	1.1313	1.1378	1.1689	**1.1720**

Multiple-Camera Tracking Scenario (MCTS),[2] [50], [51] are used in our experiments. There are a total of 265 persons and 9031 images. The correlation coefficient is used to describe the similarity between two descriptors. Table II gives the average similarities of the images within the same class and between different classes which are denoted as Υ_w and Υ_b. The ratios of two similarities are also given.

From Table II, we can find that QLRBP_4 has the best within-class similarity, while QLRBP_2 has the worst one. The within-class similarities of QLRBP_3 and QLRBP_4 are higher than those of QLRBP_1 and QLRBP_2. These results demonstrate that the fixed reference quaternions can achieve a higher similarity in within-class. On the other hand, considering the similarity between-classes, the results of QLRBP_3 and QLRBP_4 are similar, and QLRBP_2 achieves the best result. QLRBP_1 and QLRBP_2 are based on adaptive reference quaternions.

[2]http://www.eecs.qmul.ac.uk/~jason/

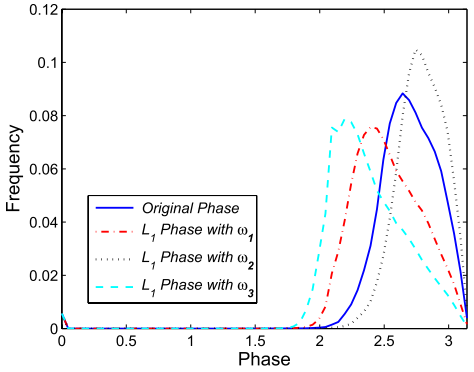

Fig. 4. Phase histograms derived by different phases of quaternions, including the original phase in Eq. (4) and the weighted L_1 phase in Eq. (6). The weights are set as follows: $\boldsymbol{\omega}_1 = \{1, 1, 1\}$, $\boldsymbol{\omega}_2 = \{0.4, 0.5, 0.6\}$, and $\boldsymbol{\omega}_3 = \{1.3, 1.4, 1.5\}$, respectively.

The reference quaternions of QLRBP_1 are derived using the vector representation of the image, while those of QLRBP_2 are obtained by QR. Compared with QLRBP_2, QLRBP_1 works better in within-class similarity, but worse in between-class similarity. Considering two similarities together, namely their ratios, the performances of QLRBP_1 and QLRBP_2 are almost the same.

The results also show that QLRBP_3 and QLRBP_4, which are derived using the fixed and orthogonal reference quaternions, achieve better performance than QLRBP_1 and QLRBP_2. The reason lies in that ReQ_1 and ReQ_2 are both clusters of the original color image and may be close to each other in the color space. Their features may contain redundant information. This problem can be solved by considering fixed and orthogonal reference quaternions. Because ReQ_4 considers more information among color channels than ReQ_3, QLRBP_4 obtains the most satisfactory performance. Therefore, ReQ_4 is used in the following experiments.

2) Weight Selection: We first study how $\boldsymbol{\omega}$ effects the value of δ. To this end, the phase histograms of images in the two person image sets (ETHZ and i-LIDS MCTS) are used to show the distribution of δ with different $\boldsymbol{\omega}$. We first perform CTQ to each image using a random unit quaternion, then compute the phase based on Eqs. (4) and (6). The weights in Eq. (6) are set to $\boldsymbol{\omega}_1 = \{1, 1, 1\}$, $\boldsymbol{\omega}_2 = \{0.4, 0.5, 0.6\}$, and $\boldsymbol{\omega}_3 = \{1.3, 1.4, 1.5\}$, respectively. The average histogram of all images for each $\boldsymbol{\omega}$ is calculated and plotted in Fig. 4. We can observe that most values of δ fall into $[\frac{\pi}{2}, \pi]$. The histogram with a large $\boldsymbol{\omega}$ has a scattered distribution, while the histogram with a small $\boldsymbol{\omega}$ has a concentrated distribution. Therefore, we can change the value range of δ by selecting a proper $\boldsymbol{\omega}$.

Next, we investigate the QLRBP coding results using different weights. The reference quaternions are chosen as ReQ_4 because it achieves the best results with the same weights. The datasets are the same as the previous experiments, and the ratio of Υ_w/Υ_b is used to evaluate the performance of each weight combination. If we set the weights to $\{1, 1, 1\}$, the ratio is 1.1720, while the ratio is 1.1718 if we use the original phase in Eq. (4). These results indicate that the use of L_1-norm can improve the performance of the original L_2-norm. In this work, we empirically set the weights

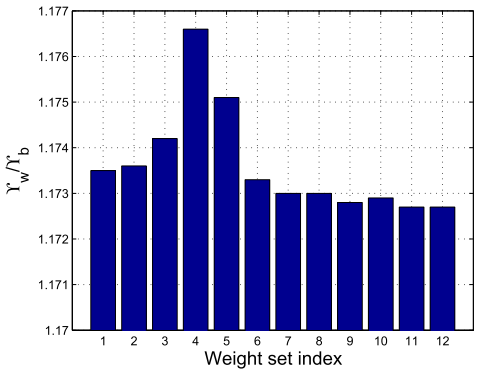

Fig. 5. The similarity ratios of the images within the same class and between different classes using different weight settings.

Fig. 6. Person image examples with appearance changes.

as follows: $\{0.1, 0.2, 0.3\}$, $\{0.2, 0.3, 0.4\}, \cdots, \{1.2, 1.3, 1.4\}$. In total, 12 sets of weights are tested here. The results are illustrated in Fig. 5. We can find that QLRBP with small weights performs better than those with large weight values. The results in Fig. 5 also show that the setting $\{0.4, 0.5, 0.6\}$ achieves the best result, and it is used in following experiments.

B. Person Reidentification

Person reidentificaiton is to identify the persons observed in nonoverlapping visual surveillance systems. It is a challenging task and many problems still remain unsolved. The main reason may lie in that there usually exists a great variance of a person's appearance in the images obtained by different nonoverlapping cameras. Fig. 6 shows several images captured from real complex environments. Images in each column contain the same person. However, it is difficult to decide whether two images are with the same person due to the synthetic effects of the view angle, lighting, occlusion, and background clutter, etc. Many local descriptors have been used for person reidentification such as the dense LBP, HOG descriptors, and dense Gabor features. Here, we evaluate QLRBP using this challenging problem. Two datasets ETHZ and i-LIDS MCTS are selected for evaluation. All images are normalized to the size of 128×64 before extracting the descriptors.

The proposed QLRBP is compared with several LBP-based descriptors and other local descriptors. They include the traditional LBP [33], robust LBP (RLBP) [52], completed LBP (CLBP) [15], upper LBP (ULBP) [46], lower LBP (LLBP) [46], and local color vector binary pattern (LCVBP) [16]. For LBP, RLBP, CLBP, LLBP, and ULBP, the descriptors are extracted from the red, green, and blue components respectively. The LCVBP descriptor is derived from the vector representation. The histograms of oriented gradient (HOG) descriptor [34] and Zheng's method [53] are also considered in our experiments. The HOG descriptor is extracted from all color channels. The Zheng's method extracts features from both the color and texture information of the original images, and the obtained features are available online.[3]

Experiments are set in the following way [53]: all images of N persons are randomly chosen from the original dataset to form a test set, which is further divided into a gallery set and a probe set. Note that there is one image for each person in the gallery set, and the rest images form the probe set. Two images are considered to be the same person if their descriptors have the smallest l_1-norm distance [54]. The average cumulative match characteristic (CMC) [53] is used to illustrate the ranked matching rates over 10 times of the repeated matching. A matching rate of the top rank score r means that the correct reidentification is obtained from the top r ranks with respect to N gallery images.

1) i-LIDS MCTS Dataset: The i-LIDS MCTS dataset was obtained indoor at an airport arrival hall. This dataset is composed of 476 images and 119 persons. These images are captured by multiple nonoverlapping cameras for each person.

Fig. 7 shows the CMC curves of $N = 30, 60, 90$ with different rank scores for all methods respectively. The quantitative results with the corresponding person numbers are given in Table III. For the results of $N = 30$, when r equals to 1, QLRBP, LCVBP, and HOG obtain more satisfactory matching results. QLRBP outperforms LCVBP and HOG about 3%, while the Zheng's method gets the worst results. As the top rank score increases, the matching rate of all methods increases. The proposed QLRBP is superior to other methods. For the largest top rank score ($r = 20, 25$), the differences of the matching rates of all methods are small. When the numbers of persons in the test set are 60 and 90, the results are different from those of $N = 30$. From the results in Fig. 7, we find that there are several layers in Figs. 7(b) and (c). QLRBP and LCVBP are on the topside, HOG, CLBP, LBP, LLBP, and ULBP are in the center layer, and the rest methods are the bottom layer. In most cases, QLRBP is about 2% higher than LCVBP.

2) ETHZ Dataset: This dataset contains three parts which are extracted from three video sequences. The numbers of persons in each part are 83, 35, 28, and the total numbers of images are 4857, 1961, 1762, respectively. Our experiments are implemented on the first part (denoted as *ETHZ1*) and a combination of other two parts (denoted as *ETHZ2* + *ETHZ3*). Figs. 8(a) and (b) show the CMC curves of $N = 30$ and $N = 60$ with different rank scores for *ETHZ1*, and Figs. 8(c) and (d) are corresponding results for $ETHZ2 + ETHZ3$. The quantitative results with the corresponding person numbers are given in Table IV. In this situation, QLRBP and LCVBP are still in a leading space and

[3]http://www.eecs.qmul.ac.uk/~jason/ilids.html.

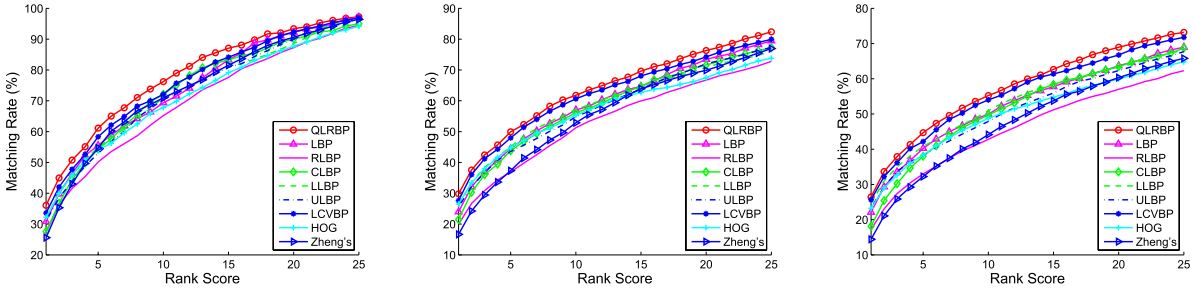

Fig. 7. CMC results of different feature extraction methods on the i-LIDS MCTS. (a) $N = 30$. (b) $N = 60$. (c) $N = 90$.

TABLE III
TOP RANKED MATCHING RATE (PERCENT) ON i-LIDS MCTS

Methods	$N = 30$					$N = 60$					$N = 90$				
	r=1	r=5	r=10	r=15	r=20	r=1	r=5	r=10	r=15	r=20	r=1	r=5	r=10	r=15	r=20
LBP	30.83	55.52	69.35	83.26	92.21	23.98	44.45	57.02	64.69	73.45	22.13	40.25	49.97	57.74	63.71
RLBP	27.31	50.16	65.22	77.62	87.26	19.97	36.88	51.27	59.97	66.72	17.23	33.00	42.81	51.19	57.02
CLBP	27.60	54.31	72.12	83.32	90.06	21.47	43.79	56.16	64.61	71.65	18.13	38.00	49.81	58.38	63.43
LLBP	31.68	54.77	71.01	81.19	88.61	26.04	45.11	57.20	64.24	70.83	24.63	40.84	50.95	58.54	63.11
ULBP	30.97	52.97	70.40	80.90	90.11	25.62	43.57	54.84	63.78	72.02	23.41	38.29	47.89	55.96	62.34
LCVBP	33.56	58.31	72.11	84.13	92.33	27.63	47.97	60.62	68.06	74.25	25.66	42.18	54.01	61.38	66.75
HOG	32.23	54.05	67.82	79.11	87.72	26.51	44.85	55.33	62.67	67.47	23.23	38.32	48.75	54.77	59.93
Zheng's	25.60	54.70	70.96	81.54	90.61	16.65	37.32	52.87	63.91	69.90	14.41	32.24	44.14	53.73	60.35
QLRBP	**36.09**	**61.13**	**76.21**	**87.05**	**93.40**	**29.82**	**49.93**	**61.78**	**69.61**	**76.31**	**26.45**	**44.69**	**55.23**	**62.65**	**68.95**

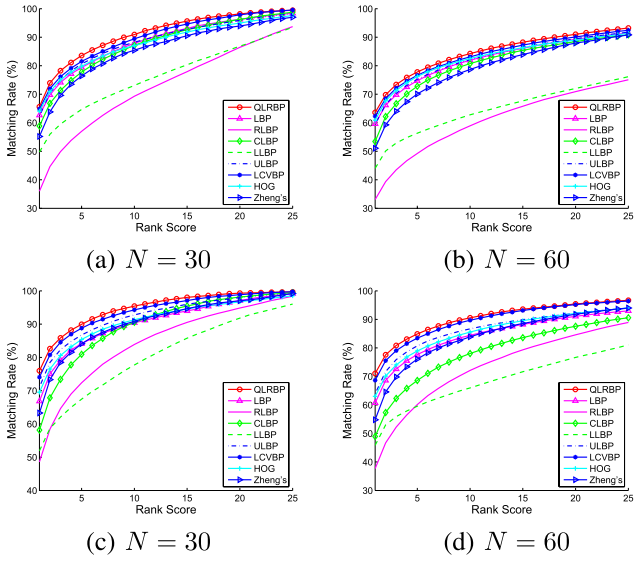

Fig. 8. CMC results of different feature extraction methods on the ETHZ. (a) and (b) are results of $ETHZ1$, and (c) and (d) are results of $ETHZ2 + ETHZ3$.

achieve more satisfactory results. LLBP and RLBP may not be suitable for the ETHZ datase because their matching rates are much lower than those of other methods. Generally speaking, QLRBP performs slightly better than LCVBP in most cases.

C. Color Face Recognition

Face recognition is one successful and popular application for the LBP-based descriptors. Here, we experimentally evaluate the proposed QLRBP using the color face recognition problem. We use three public color face databases, namely NUST Real-world face recognition (RWFR) database,[4] AR database [55], [56], and SCface database [57]. NUST RWFR contains the color face images of 100 persons and 24 images for each person. In RWFR, the images for each person can be divided into two sections. The first section contains 12 images with high quality, while the rest images are acquired under poor conditions (like low contrast, blur, or shadow). The cropped AR face database includes 2600 color images corresponding to 50 men and 50 women, and the images for each person contain large varieties of facial expressions, illumination, and occlusion. SCface database consists of 4160 static face images of 130 subjects, and these images were taken in uncontrolled environments by several video surveillance cameras of various qualities. 2080 images are selected from the whole database to evaluate the performance of QLRBP against low resolution as in [16] and [57].

The face recognition here is also implemented as the person reidentification problem. The LBP-based methods used in Section VI-B are also selected for comparison here. Table V shows the results of all methods when N is set to be 30, 60, and 90 respectively. From these results we can find that LCVBP and QLRBP obviously outperform other LBP-based methods in the NUST RWFR and AR databases, and achieve much better improvements as the image number in the testing set increases. In these situations, when the top ranking number r is small, the matching rates of LCVBP and QLRBP are almost the same. As r increases, the matching rates of QLRBP are about one or two percents larger than those of LCVBP in

[4]http://pcalab.njust.edu.cn/

TABLE IV
TOP RANKED MATCHING RATE (PERCENT) ON ETHZ

ETHZ 1												
Methods	$N = 30$						$N = 60$					
	r=1	r=5	r=10	r=15	r=20	r=25	r=1	r=5	r=10	r=15	r=20	r=25
LBP	62.65	79.36	87.85	93.09	96.24	98.39	59.62	74.75	81.91	86.09	89.26	91.50
RLBP	35.97	57.00	69.31	77.90	86.45	93.73	33.05	49.24	58.92	65.78	70.93	75.08
CLBP	58.85	77.77	87.12	92.66	96.25	98.79	53.44	72.80	80.75	85.39	88.48	90.84
LLBP	49.74	64.66	73.08	80.32	86.89	93.50	44.02	56.33	62.78	67.66	72.04	76.16
ULBP	62.33	80.63	88.24	92.82	95.90	98.35	59.44	75.23	82.12	86.39	89.44	91.79
LCVBP	64.85	81.52	89.45	94.64	97.87	**99.57**	62.30	76.64	83.12	87.22	90.10	92.42
HOG	64.10	79.83	87.07	91.81	94.96	97.62	60.90	76.24	82.51	86.31	88.95	91.33
Zheng's	55.20	76.41	85.44	90.52	93.93	97.02	51.06	70.08	78.69	83.91	87.94	90.81
QLRBP	**65.63**	**83.57**	**90.91**	**95.65**	**98.16**	99.44	**63.60**	**77.79**	**84.25**	**88.22**	**91.01**	**93.21**

ETHZ 2 + ETHZ 3												
Methods	$N = 30$						$N = 60$					
	r=1	r=5	r=10	r=15	r=20	r=25	r=1	r=5	r=10	r=15	r=20	r=25
LBP	66.84	84.13	90.42	93.98	97.06	99.14	60.71	77.65	84.41	88.23	91.07	92.99
RLBP	48.57	72.37	83.90	90.53	94.86	98.39	37.67	60.13	72.10	79.33	84.58	88.93
CLBP	58.15	80.94	90.55	95.46	98.16	99.43	48.92	68.57	78.04	83.59	87.59	90.57
LLBP	51.93	67.47	77.72	85.77	91.82	96.03	45.84	59.57	65.97	71.65	76.65	81.06
ULBP	71.11	86.73	92.78	95.97	97.99	99.27	63.95	80.72	86.67	89.90	92.11	93.92
LCVBP	74.05	88.78	94.29	97.08	98.86	**99.74**	68.66	83.44	89.70	93.12	95.17	96.42
HOG	69.55	85.39	91.32	94.57	96.72	98.53	63.01	78.93	85.53	89.55	92.09	94.00
Zheng's	63.29	84.10	90.84	94.67	97.02	99.19	54.79	76.10	83.88	88.57	91.79	94.00
QLRBP	**75.98**	**89.94**	**95.41**	**98.03**	**99.31**	99.69	**71.03**	**84.87**	**90.54**	**93.56**	**95.41**	**96.69**

TABLE V
TOP RANKED MATCHING RATE (PERCENT) ON FACE DATASETS. (a) NUST RWFR FACE DATASET. (b) AR FACE DATASET. (c) SCFACE DATASET

(a)															
Methods	$N = 30$					$N = 60$					$N = 90$				
	r=1	r=5	r=10	r=15	r=20	r=1	r=5	r=10	r=15	r=20	r=1	r=5	r=10	r=15	r=20
LBP	29.64	51.74	66.59	77.61	86.12	24.01	40.78	51.86	60.20	67.07	21.85	35.97	45.02	51.75	57.18
RLBP	27.03	51.16	67.61	79.19	87.46	21.81	39.70	51.20	59.88	66.49	19.59	34.76	44.46	51.31	56.71
CLBP	27.41	50.72	65.51	75.94	84.20	20.32	37.42	48.41	57.09	63.73	18.96	33.28	42.45	49.14	54.85
LLBP	27.06	48.26	61.68	72.54	81.74	20.54	36.05	47.51	55.04	61.55	18.87	31.46	40.10	46.59	51.73
ULBP	25.91	47.68	61.52	72.50	81.17	20.02	35.62	46.49	54.03	61.07	18.25	30.55	39.05	45.48	50.90
LCVBP	32.33	55.81	70.46	79.90	87.71	26.41	44.25	55.59	63.77	70.18	25.02	40.28	49.55	56.31	61.49
QLRBP	**34.14**	**58.01**	**72.57**	**81.71**	**89.63**	**27.82**	**46.61**	**57.63**	**65.42**	**71.97**	**25.80**	**41.71**	**51.76**	**58.48**	**63.55**

(b)															
Methods	$N = 30$					$N = 60$					$N = 90$				
	r=1	r=5	r=10	r=15	r=20	r=1	r=5	r=10	r=15	r=20	r=1	r=5	r=10	r=15	r=20
LBP	19.07	37.84	55.79	69.27	83.01	15.77	27.92	40.24	49.51	56.77	14.12	23.96	32.49	40.27	46.66
RLBP	16.88	35.37	53.31	66.71	80.44	14.07	25.43	36.97	45.98	53.48	12.14	21.42	30.02	37.28	43.58
CLBP	16.64	38.88	58.76	74.97	86.21	13.05	27.05	38.61	49.01	58.38	11.01	21.98	31.25	38.88	45.52
LLBP	18.87	41.82	61.15	76.16	86.48	14.65	29.27	42.66	53.07	60.82	13.16	24.60	34.84	43.25	50.49
ULBP	19.16	42.57	61.55	75.92	86.73	15.49	29.35	42.95	52.75	60.93	13.73	24.79	35.17	43.87	50.80
LCVBP	22.59	44.86	62.15	74.57	85.57	18.25	34.35	47.33	55.99	62.72	15.80	29.65	39.72	47.52	53.35
QLRBP	**23.49**	**47.47**	**65.37**	**78.00**	**87.60**	**19.05**	**36.43**	**49.67**	**58.55**	**65.56**	**16.52**	**31.10**	**41.57**	**49.73**	**55.69**

(c)															
Methods	$N = 30$					$N = 60$					$N = 90$				
	r=5	r=10	r=15	r=20	r=25	r=5	r=10	r=15	r=20	r=25	r=5	r=10	r=15	r=20	r=25
LBP	30.93	45.33	58.51	72.93	88.36	**24.41**	31.98	38.29	45.23	52.22	**20.76**	26.87	31.44	36.32	41.16
RLBP	29.49	45.67	58.64	71.76	86.96	21.08	30.41	38.89	46.46	53.07	16.65	24.53	30.76	36.67	41.57
CLBP	25.87	40.73	55.89	71.42	86.84	18.76	26.79	35.02	42.22	49.86	14.95	20.94	26.56	31.93	36.95
LLBP	31.71	47.76	62.13	75.84	88.57	22.72	32.26	40.43	48.01	54.53	19.68	26.78	32.57	37.99	43.51
ULBP	32.09	47.36	63.04	76.00	88.35	23.39	32.20	39.68	47.09	54.11	19.98	**27.61**	33.44	38.49	43.47
LCVBP	32.53	48.97	62.51	75.84	88.84	22.47	32.62	40.78	48.71	55.66	18.04	26.34	32.76	38.46	44.20
QLRBP	**34.07**	**49.42**	**63.13**	**76.42**	**89.02**	23.38	**33.90**	**42.02**	**49.48**	**56.22**	18.48	27.14	**33.82**	**39.75**	**45.00**

most cases. It is more challenging to extract robust descriptors from the SCface database because of the low resolution of images. LLBP, ULBP, LCVBP, and QLRBP obtain more satisfactory results. QLRBP achieves the best performance in most cases. The results demonstrate the effectiveness and superiority of QLRBP.

The face images of the same person in the experiments exist large variations in expression, illumination, or pose. The performance of QLRBP surpasses those of other LBP-based methods. The reasons lie in following aspects: First, the use of different reference quaternions make the derived feature more comprehensive. The CTQ operation between the QR and reference quaternion reveals the specific color characteristics of the original image. The three reference quaternions are able to extract sufficient discriminative features from the image. Second, QLRBP is an illumination insensitive descriptor. The features extracted from the gradient domain have been proved to be robust to illumination changes [58]. QLRBP contains similar operations. For example, $|gb' - bg'|$ in Eq. (27) is similar to the gradient calculation. In this way, the LBP coding is implemented in this color contrast domain. All these operations ensure that QLRBP is robust to illuminative variations.

VII. Conclusion

In this paper, we proposed QLRBP as a local descriptor of color images. Different from other descriptors, QLRBP is extracted from the quaternionic representation of a color image that offers another perspective of the color image. Several quaternionic operators, like rotation, phase, and Clifford translation, have been applied to process color images in the quaternionic domain. Compared with existing LBP-based methods, QLRBP considers more image characteristics and shows more robustness to different variations. Person reidentification and face recognition were selected to evaluate QLRBP. The experimental results demonstrated the effectiveness of the proposed QLRBP.

We also proposed a new understanding of several existing LBP-based methods by converting them into a scheme to determine an ordering relation, and used a ranking function to describe this relationship. The CTQ was introduced to derive the ranking function for two quaternions. We further investigated the properties of CTQ and compared it with ROQ. The phase of the CTQ image can reveal the relation of color channels. Our future work will find other quaternionic operators to design suitable ranking functions and develop other local descriptors (like SIFT, HOG) in the quaternionic domain.

Appendix

A. Proof of Property 1

Proof: $\dot{p}$ is a unit quaternion then $|\dot{p}| = 1$. Based on the modulus of the quaternion's multiplication, we have

$$|\mathrm{CTQ}_r(\dot{q}, \dot{p})| = |\dot{q}\dot{p}| = |\dot{q}||\dot{p}| = |\dot{q}|,$$
$$|\mathrm{CTQ}_l(\dot{q}, \dot{p})| = |\dot{p}\dot{q}| = |\dot{p}||\dot{q}| = |\dot{q}|.$$

Therefore, CTQ is an operator with modulus-invariant for a quaternion. ∎

B. Proof of Property 2

Proof: Suppose $\dot{q} = a_1 + b_1 i + c_1 j + d_1 k$ and $\dot{p} = a_2 + b_2 i + c_2 j + d_2 k$ ($\dot{q} \neq \dot{p}$), we have

$$\mathrm{CTQ}_r(\dot{q}, \dot{p}) = \dot{q}\dot{p} \triangleq a_3 + b_3 i + c_3 j + d_3 k, \tag{31}$$

where $a_3 = a_1a_2 - b_1b_2 - c_1c_2 - d_1d_2, b_3 = a_1b_2 + b_1a_2 + c_1d_2 - d_1c_2, c_3 = a_1c_2 - b_1d_2 + c_1a_2 + d_1b_2, d_3 = a_1d_2 + b_1c_2 - c_1b_2 + d_1a_2$. Similarly, it has

$$\mathrm{CTQ}_l(\dot{q}, \dot{p}) = \dot{p}\dot{q} \triangleq a_4 + b_4 i + c_4 j + d_4 k, \tag{32}$$

where $a_4 = a_2a_1 - b_2b_1 - c_2c_1 - d_2d_1, b_4 = a_2b_1 + b_2a_1 + c_2d_1 - d_2c_1, c_4 = a_2c_1 - b_2d_1 + c_2a_1 + d_2b_1, d_4 = a_2d_1 + b_2c_1 - c_2b_1 + d_2a_1$.

It is not difficult to see $a_3 = a_4$, but $b_3 \neq b_4, c_3 \neq c_4$, $d_3 \neq d_4$. Therefore, $\mathrm{CTQ}_r(\dot{q}, \dot{p}) \neq \mathrm{CTQ}_l(\dot{q}, \dot{p})$ but their real parts are the same.

Based on Property 1 and the modulus of a quaternion, we can obtain

$$b_3^2 + c_3^2 + d_3^2 = b_4^2 + c_4^2 + d_4^2. \tag{33}$$

According to the phase definition,

$$\theta_{\mathrm{CTQ}_r(\dot{q},\dot{p})} = \frac{\sqrt{b_3^2 + c_3^2 + d_3^2}}{a_3},$$
$$\theta_{\mathrm{CTQ}_l(\dot{q},\dot{p})} = \frac{\sqrt{b_4^2 + c_4^2 + d_4^2}}{a_4}.$$

From above equations, we can find that $\theta_{\mathrm{CTQ}_r(\dot{q},\dot{p})} = \theta_{\mathrm{CTQ}_l(\dot{q},\dot{p})}$ using $a_3 = a_4$ and Eq. (33). ∎

C. Proof of Property 3

Proof: According to the definitions of ROQ and CTQ, we have

$$\begin{aligned}\mathrm{CTQ}_r(\mathrm{CTQ}_l(\dot{q}, \dot{p}), \dot{p}^*) &= \mathrm{CTQ}_r(\dot{p}\dot{q}, \dot{p}^*) \\ &= \dot{p}\dot{q}\dot{p}^* = \mathrm{ROQ}(\dot{q}, \dot{p}), \\ \mathrm{CTQ}_l(\mathrm{CTQ}_r(\dot{q}, \dot{p}^*), \dot{p}) &= \mathrm{CTQ}_l(\dot{q}\dot{p}^*, \dot{p}) \\ &= \dot{p}\dot{q}\dot{p}^* = \mathrm{ROQ}(\dot{q}, \dot{p}).\end{aligned}$$

Therefore, ROQ can be implemented using CTQ. ∎

D. Proof of Property 4

Proof: Suppose $\dot{q} = b_1 i + c_1 j + d_1 k$ and $\dot{p} = b_2 i + c_2 j + d_2 k$ ($\dot{q} \neq \dot{p}$), we have

$$\mathrm{CTQ}_r(\dot{q}, \dot{p}) = \dot{q}\dot{p} \triangleq a_3 + b_3 i + c_3 j + d_3 k, \tag{34}$$

where $a_3 = -b_1b_2 - c_1c_2 - d_1d_2, b_3 = c_1d_2 - d_1c_2, c_3 = -b_1d_2 + d_1b_2, d_3 = b_1c_2 - c_1b_2$.

Similarly,

$$\mathrm{CTQ}_l(\dot{q}, \dot{p}) = \dot{p}\dot{q} \triangleq a_4 + b_4 i + c_4 j + d_4 k, \tag{35}$$

where $a_4 = -b_2b_1 - c_2c_1 - d_2d_1, b_4 = c_2d_1 - d_2c_1, c_4 = -b_2d_1 + d_2b_1, d_4 = b_2c_1 - c_2b_1$. We can find that

$$a_3 = a_4, \text{ and } b_3 i + c_3 j + d_3 k = -(b_4 i + c_4 j + d_4 k).$$

Thus, $\mathrm{CTQ}_r(\dot{q}, \dot{p}) = \mathrm{CTQ}_l(\dot{q}, \dot{p})^*$. ∎

E. Proof of Property 5

Proof: The notations used in the proof of Property 4 are considered here. From Eqs. (34) and (35), we know that: $a_3 = a_4, b_3 = -b_4, c_3 = -c_4$, and $d_3 = -d_4$. Combining these results with the definition of the weighted L_1 phase, we can derive the desired result. ∎

ACKNOWLEDGEMENTS

The authors would like to thank the anonymous reviewers for their valued comments and constructive suggestions that significantly improved the quality of this paper.

REFERENCES

[1] M.-K. Hu, "Visual pattern recognition by moment invariants," *IRE Trans. Inf. Theory*, vol. 8, no. 2, pp. 179–187, Feb. 1962.
[2] T. P. Wallace and P. A. Wintz, "An efficient three-dimensional aircraft recognition algorithm using normalized Fourier descriptors," *Comput. Graph. Image Process.*, vol. 13, no. 2, pp. 99–126, 1980.
[3] G. C.-H. Chuang and C.-C. J. Kuo, "Wavelet descriptor of planar curves: Theory and applications," *IEEE Trans. Image Process.*, vol. 5, no. 1, pp. 56–70, Jan. 1996.
[4] I. El Rube, M. Ahmed, and M. Kamel, "Wavelet approximation-based affine invariant shape representation functions," *IEEE Trans. Pattern Anal. Mach. Intell.*, vol. 28, no. 2, pp. 323–327, Feb. 2006.
[5] R. Mukundan, S. H. Ong, and P. A. Lee, "Image analysis by Tchebichef moments," *IEEE Trans. Image Process.*, vol. 10, no. 9, pp. 1357–1364, Sep. 2001.
[6] H. Zhang, H. Shu, G. N. Han, G. Coatrieux, L. Luo, and J. L. Coatrieux, "Blurred image recognition by Legendre moment invariants," *IEEE Trans. Image Process.*, vol. 19, no. 3, pp. 596–611, Mar. 2010.
[7] G. Liu, Z. Lin, and Y. Yu, "Radon representation-based feature descriptor for texture classification," *IEEE Trans. Image Process.*, vol. 18, no. 5, pp. 921–928, May 2009.
[8] R. Lan and J. Yang, "Orthogonal projection transform with application to shape description," in *Proc. 17th IEEE Int. Conf. Image Process. (ICIP)*, Sep. 2010, pp. 281–284.
[9] R. Lan, J. Yang, Y. Jiang, C. Fyfe, and Z. Song, "Whitening central projection descriptor for affine-invariant shape description," *IET Image Process.*, vol. 7, no. 1, pp. 81–91, 2013.
[10] D. G. Lowe, "Distinctive image features from scale-invariant keypoints," *Int. J. Comput. Vis.*, vol. 60, no. 2, pp. 91–110, 2004.
[11] H. Bay, T. Tuytelaars, and L. Van Gool, "SURF: Speeded up robust features," in *Proc. Eur. Conf. Comput. Vis. (ECCV)*, 2006, pp. 404–417.
[12] J.-M. Morel and G. Yu, "ASIFT: A new framework for fully affine invariant image comparison," *SIAM J. Imag. Sci.*, vol. 2, no. 2, pp. 438–469, 2009.
[13] J.-M. Guo and H. Prasetyo, "Content-based image retrieval using features extracted from halftoning-based block truncation coding," *IEEE Trans. Image Process.*, vol. 24, no. 3, pp. 1010–1024, Mar. 2015.
[14] J. Li, X. Li, B. Yang, and X. Sun, "Segmentation-based image copy-move forgery detection scheme," *IEEE Trans. Inf. Forensics Security*, vol. 10, no. 3, pp. 507–518, Mar. 2015.
[15] Z. Guo and D. Zhang, "A completed modeling of local binary pattern operator for texture classification," *IEEE Trans. Image Process.*, vol. 19, no. 6, pp. 1657–1663, Jan. 2010.
[16] S. H. Lee, J. Y. Choi, Y. M. Ro, and K. N. Plataniotis, "Local color vector binary patterns from multichannel face images for face recognition," *IEEE Trans. Image Process.*, vol. 21, no. 4, pp. 2347–2353, Apr. 2012.
[17] S. J. Sangwine, "Fourier transforms of colour images using quaternion or hypercomplex, numbers," *Electron. Lett.*, vol. 32, no. 21, pp. 1979–1980, 1996.
[18] S.-C. Pei and C.-M. Cheng, "Color image processing by using binary quaternion-moment-preserving thresholding technique," *IEEE Trans. Image Process.*, vol. 8, no. 5, pp. 614–628, May 1999.
[19] T. A. Ell and S. J. Sangwine, "Hypercomplex Fourier transforms of color images," *IEEE Trans. Image Process.*, vol. 16, no. 1, pp. 22–35, Jan. 2007.
[20] E. G. Karakasis, G. G. Papakostas, D. E. Koulouriotis, and V. D. Tourassis, "A unified methodology for computing accurate quaternion color moments and moment invariants," *IEEE Trans. Image Process.*, vol. 23, no. 2, pp. 596–611, Feb. 2014.
[21] P. Denis, P. Carre, and C. Fernandez-Maloigne, "Spatial and spectral quaternionic approaches for colour images," *Comput. Vis. Image Understand.*, vol. 107, nos. 1–2, pp. 74–87, 2007.
[22] C. E. Moxey, S. J. Sangwine, and T. A. Ell, "Hypercomplex correlation techniques for vector images," *IEEE Trans. Signal Process.*, vol. 51, no. 7, pp. 1941–1953, Jul. 2003.
[23] T. K. Paul and T. Ogunfunmi, "A kernel adaptive algorithm for quaternion-valued inputs," *IEEE Trans. Neural Netw. Learn. Syst.*, vol. 26, no. 10, pp. 2422–2439, Oct. 2015.
[24] L.-Q. Guo and M. Zhu, "Quaternion Fourier–Mellin moments for color images," *Pattern Recognit.*, vol. 44, no. 2, pp. 187–195, 2011.
[25] J.-C. Souyris and C. Tison, "Polarimetric analysis of bistatic SAR images from polar decomposition: A quaternion approach," *IEEE Trans. Geosci. Remote Sens.*, vol. 45, no. 9, pp. 2701–2714, Sep. 2007.
[26] A. Kolaman and O. Yadid-Pecht, "Quaternion structural similarity: A new quality index for color images," *IEEE Trans. Image Process.*, vol. 21, no. 4, pp. 1526–1536, Apr. 2012.
[27] B. Chen, H. Shu, H. Zhang, G. Chen, and L. Luo, "Color image analysis by quaternion Zernike moments," in *Proc. 20th IEEE Int. Conf. Pattern Recognit. (ICPR)*, 2010, pp. 625–628.
[28] B. J. Chen *et al.*, "Quaternion Zernike moments and their invariants for color image analysis and object recognition," *Signal Process.*, vol. 92, no. 2, pp. 308–318, 2012.
[29] J. Mennesson, C. Saint-Jean, and L. Mascarilla, "New geometric Fourier descriptors for color image recognition," in *Proc. 17th IEEE Int. Conf. Image Process. (ICIP)*, Sep. 2010, pp. 2685–2688.
[30] Z. Yang and S.-I. Kamata, "Hypercomplex polar Fourier analysis for color image," in *Proc. 18th IEEE Int. Conf. Image Process. (ICIP)*, Sep. 2011, pp. 2117–2120.
[31] Y. Xu, "Quaternion-based discriminant analysis method for color face recognition," *PloS One*, vol. 7, no. 8, p. e43493, 2012.
[32] K. Mikolajczyk and C. Schmid, "A performance evaluation of local descriptors," *IEEE Trans. Pattern Anal. Mach. Intell.*, vol. 27, no. 10, pp. 1615–1630, Oct. 2005.
[33] T. Ojala, M. Pietikäinen, and T. Mäenpää, "Multiresolution gray-scale and rotation invariant texture classification with local binary patterns," *IEEE Trans. Pattern Anal. Mach. Intell.*, vol. 24, no. 7, pp. 971–987, Jul. 2002.
[34] N. Dalal and B. Triggs, "Histograms of oriented gradients for human detection," in *Proc. IEEE Conf. Comput. Vis. Pattern Recognit. (CVPR)*, Jun. 2005, pp. 886–893.
[35] Y. Li, W. Liu, X. Li, Q. Huang, and X. Li, "GA-SIFT: A new scale invariant feature transform for multispectral image using geometric algebra," *Inf. Sci.*, vol. 281, pp. 559–572, Oct. 2014.
[36] J. Chen, S. Shan, G. Zhao, X. Chen, W. Gao, and M. Pietikäinen, "A robust descriptor based on Weber's law," in *Proc. IEEE Conf. Comput. Vis. Pattern Recognit. (CVPR)*, Jun. 2008, pp. 1–7.
[37] J. Chen *et al.*, "WLD: A robust local image descriptor," *IEEE Trans. Pattern Anal. Mach. Intell.*, vol. 32, no. 9, pp. 1705–1720, Sep. 2010.
[38] J. van de Weijer, T. Gevers, and A. D. Bagdanov, "Boosting color saliency in image feature detection," *IEEE Trans. Pattern Anal. Mach. Intell.*, vol. 28, no. 1, pp. 150–156, Jan. 2006.
[39] A. Bosch, A. Zisserman, and X. Muñoz, "Scene classification using a hybrid generative/discriminative approach," *IEEE Trans. Pattern Anal. Mach. Intell.*, vol. 30, no. 4, pp. 712–727, Apr. 2008.
[40] D. Gray and H. Tao, "Viewpoint invariant pedestrian recognition with an ensemble of localized features," in *Proc. 10th Eur. Conf. Comput. Vis. (ECCV)*, 2008, pp. 262–275.
[41] W. Lu, Y. Xu, X. Yang, and L. Song, "Local quaternionic Gabor binary patterns for color face recognition," in *Proc. IEEE Int. Conf. Acoust., Speech Signal Process. (ICASSP)*, Mar./Apr. 2008, pp. 741–744.
[42] G. J. Burghouts and J.-M. Geusebroek, "Performance evaluation of local colour invariants," *Comput. Vis. Image Understand.*, vol. 113, no. 1, pp. 48–62, 2009.
[43] K. E. A. van de Sande, T. Gevers, and C. G. M. Snoek, "Evaluating color descriptors for object and scene recognition," *IEEE Trans. Pattern Anal. Mach. Intell.*, vol. 32, no. 9, pp. 1582–1596, Sep. 2010.
[44] W. R. Hamilton, *Elements of Quaternions*. London, U.K.: Longmans Green, 1866.
[45] J. Weeks, R. Lehoucq, and J.-P. Uzan, "Detecting topology in a nearly flat spherical universe," *Classical Quantum Gravity*, vol. 20, no. 8, p. 1529, 2003.
[46] X. Tan and B. Triggs, "Enhanced local texture feature sets for face recognition under difficult lighting conditions," *IEEE Trans. Image Process.*, vol. 19, no. 6, pp. 1635–1650, Jun. 2010.
[47] Z. Cao, Q. Yin, X. Tang, and J. Sun, "Face recognition with learning-based descriptor," in *Proc. IEEE Conf. Comput. Vis. Pattern Recognit. (CVPR)*, Jun. 2010, pp. 2707–2714.
[48] Y. Huang, Z. Wu, L. Wang, and T. Tan, "Feature coding in image classification: A comprehensive study," *IEEE Trans. Pattern Anal. Mach. Intell.*, vol. 36, no. 3, pp. 493–506, Mar. 2014.
[49] A. Ess, B. Leibe, and L. Van Gool, "Depth and appearance for mobile scene analysis," in *Proc. IEEE 11th Int. Conf. Comput. Vis. (ICCV)*, Oct. 2007, pp. 1–8.
[50] *i-LIDS Multiple Camera Tracking Scenario Definition*, UK Home Office, Lodon, U.K., 2008.

[51] W.-S. Zheng, S. Gong, and T. Xiang, "Associating groups of people," in *Proc. Brit. Mach. Vis. Conf.*, 2009, pp. 23.1–23.11.
[52] D. T. Nguyen, Z. Zong, P. Ogunbona, and W. Li, "Object detection using non-redundant local binary patterns," in *Proc. 17th IEEE Int. Conf. Image Process. (ICIP)*, Sep. 2010, pp. 4609–4612.
[53] W.-S. Zheng, S. Gong, and T. Xiang, "Reidentification by relative distance comparison," *IEEE Trans. Pattern Anal. Mach. Intell.*, vol. 35, no. 3, pp. 653–668, Mar. 2013.
[54] X. Wang, G. Doretto, T. Sebastian, J. Rittscher, and P. Tu, "Shape and appearance context modeling," in *Proc. 11th IEEE Int. Conf. Comput. Vis. (ICCV)*, Oct. 2007, pp. 1–8.
[55] A. M. Martínez and R. Benavente, "The AR face database," CVC, Barcelona, Spain, Tech. Rep. #24, 1998.
[56] A. M. Martínez and A. C. Kak, "PCA versus LDA," *IEEE Trans. Pattern Anal. Mach. Intell.*, vol. 23, no. 2, pp. 228–233, Feb. 2001.
[57] M. Grgic, K. Delac, and S. Grgic, "SCface—Surveillance cameras face database," *Multimedia Tools Appl.*, vol. 51, no. 3, pp. 863–879, 2011.
[58] T. Zhang, Y. Y. Tang, B. Fang, Z. Shang, and X. Liu, "Face recognition under varying illumination using gradientfaces," *IEEE Trans. Image Process.*, vol. 18, no. 11, pp. 2599–2606, Nov. 2009.

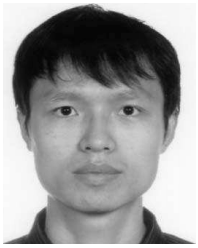

Rushi Lan received the B.S. and M.S. degrees from the Nanjing University of Information Science and Technology, Nanjing, China, in 2008 and 2011, respectively. He is currently pursuing the Ph.D. degree with the Department of Computer and Information Science, University of Macau, Macau, China.

His current research interests include image classification, image denoising, and metric learning.

Yicong Zhou (M'07–SM'14) received the B.S. degree from Hunan University, Changsha, China, in 1992, and the M.S. and Ph.D. degrees from Tufts University, Medford, MA, USA, in 2008 and 2010, respectively, all in electrical engineering.

He is currently an Assistant Professor with the Department of Computer and Information Science, University of Macau, Macau, China. His current research interests include multimedia security, image/signal processing, pattern recognition, and medical imaging.

Dr. Zhou is a member of the International Society for Photo-Optical Instrumentations Engineers and the Association for Computing Machinery. He received the third price of the Macau Natural Science Award in 2014.

Yuan Yan Tang (F'04) received the B.S. degree in electrical and computer engineering from Chongqing University, Chongqing, China, the M.S. degree in electrical engineering from the Beijing University of Post and Telecommunications, Beijing, China, and the Ph.D. degree in computer science from Concordia University, Montreal, QC, Canada.

He is currently a Chair Professor with the Faculty of Science and Technology, University of Macau, Macau, China, and a Professor/Adjunct Professor/Honorary Professor at several institutions including Chongqing University, Concordia University, and Hong Kong Baptist University, Hong Kong. He is the Founder and Editor-in-Chief of the *International Journal of Wavelets*, *Multiresolution*, and *Information Processing*, and an Associate Editor of several international journals. He has published more than 400 academic papers and has authored or co-authored over 25 monographs/books/book chapters. His current interests include wavelets, pattern recognition, and image processing.

Dr. Tang is a fellow of the International Association for Pattern Recognition (IAPR). He is the Founder and Chair of the Pattern Recognition Committee of the IEEE SMC. He has served as the General Chair, Program Chair, and Committee Member of many international conferences. He is the Founder and General Chair of the series International Conferences on Wavelets Analysis and Pattern Recognition. He is the Founder and Chair of the Macau Branch of IAPR.